2013

Uniformity of Glycyl Bridge Lengths in the Mature Cell Walls of Fem Mutants of Methicillin-Resistant Staphylococcus aureus

Shasad Sharif
Washington University in St Louis

Sung Joon Kim
Baylor University

Harald Labischinski
MerLion Pharmaceuticals GmbH

Jiawei Chen
Washington University in St Louis

Jacob Schaefer
Washington University in St Louis

Journal of Bacteriology

Uniformity of Glycyl Bridge Lengths in the Mature Cell Walls of Fem Mutants of Methicillin-Resistant Staphylococcus aureus

Shasad Sharif, Sung Joon Kim, Harald Labischinski, Jiawei Chen and Jacob Schaefer

J. Bacteriol. **2013, 195(7):1421. DOI: 10.1128/JB.01471-12.**
Published Ahead of Print 18 January 2013.

JB
Journals.ASM.org

Uniformity of Glycyl Bridge Lengths in the Mature Cell Walls of Fem Mutants of Methicillin-Resistant *Staphylococcus aureus*

Shasad Sharif,[a] Sung Joon Kim,[b] Harald Labischinski,[c] Jiawei Chen,[a] Jacob Schaefer[a]

Department of Chemistry, Washington University, St. Louis, Missouri, USA[a]; Department of Chemistry and Biochemistry, Baylor University, Waco, Texas, USA[b]; MerLion Pharmaceuticals GmbH, Berlin, Germany[c]

Peptidoglycan (PG) composition in intact cells of methicillin-resistant *Staphylococcus aureus* (MRSA) and its isogenic Fem mutants has been characterized by measuring the glycine content of PG bridge structures by solid-state nuclear magnetic resonance (NMR). The glycine content estimated from integrated intensities (rather than peak heights) in the cell walls of whole cells was increased by approximately 30% for the FemA mutant and was reduced by 25% for the FemB mutant relative to expected values for homogeneous structures. In contrast, the expected compositions were observed in isolated cell walls of the same mutants. For FemA mutant whole cells, the increase was due to the presence of triglycyl bridge PG units (confirmed directly by mass spectrometric analysis), which constituted 10% of the total PG. These species were coalesced in some sort of a lattice or aggregate with spatial proximity to other PG bridges. This result suggests that the triglycyl-bridged PG units form a PG-like structure that is not incorporated into the mature cell wall.

Peptidoglycan (PG) is an essential component of the bacterial cell wall whose biosynthesis is targeted by several classes of antibiotics, including β-lactams (1, 2) and glycopeptides (3–5). In *Staphylococcus aureus* (6), a thick cell wall consisting of 20 or more layers of glycan enables the bacteria to withstand fluctuating osmotic pressure (2). An illustrated PG lattice structure for *S. aureus* is shown in Fig. 1 (top). The repeating PG unit consists of a disaccharide [*N*-acetylglucosamine-(β_{1-4})–*N*-acetylmuramic acid (GlcNAc-MurNAc)], a pentapeptide stem (L-Ala_1–D-*iso*-Gln_2–L-Lys_3–D-Ala_4–D-Ala_5), and a pentaglycyl bridge. The PG assembly is carried out by two enzymatic processes: (i) transglycosylation that elongates disaccharides of repeating PG units to form a growing glycan backbone (2) and (ii) transpeptidation that cross-links the glycan chains from a terminal bridging glycine residue of one stem to the D-Ala_4 of an adjacent stem with the cleavage of D-Ala_5 (2). The assembled PG tertiary structure remains unknown and is currently open to debate (7, 8).

The *fem* factors (factors essential for methicillin resistance) (9–11), alternatively termed auxiliary factors (12), carry out sequential glycine additions to the PG-lysyl side chain of lipid II, the essential membrane-bound PG precursor. Presumably, FemX (13) catalyzes the addition of the first glycyl unit, FemA (8, 14) catalyzes the addition of the second and third glycyl units, and FemB (15) catalyzes the addition of the fourth and fifth glycyl units, to complete pentaglycyl bridge biosynthesis in *S. aureus*. Inactivation of *femA* by point mutagenesis (16, 17) and *femB* by transposon insertion (15) in methicillin-resistant *S. aureus* (MRSA) (18, 19) results in FemA (UK17) and FemB (UT34-2) mutants, respectively, that biosynthesize PG with mono- and triglycyl bridge structures (Fig. 1, bottom). Complete knockout of the *femA* and *femB* genes resulted in a FemAB (AS145) null mutant (14, 20, 21) having a monoglycyl bridge structure, as in the FemA mutant. An additional hidden mutation(s) acquired during the construction in the FemAB null mutant (and possibly present in FemA as well) was suggested previously by Ling and Berger-Bächi (22). So far, this hidden mutation(s) has not been linked to cell wall biosynthesis. All Fem mutants of MRSA, which carry the additional low-affinity penicillin-binding protein PBP2a (2, 12), exhibit reduced methicillin (β-lactam) resistance (9, 10) (listed in Table 1) and irregular cell morphologies (24, 25). In this report, we describe the effects of changes in glycine bridge length on the PG composition and structure for intact cells of MRSA and its isogenically derived Fem mutants.

We proposed previously a template model to explain the high levels of cross-linking of the PG in *S. aureus* (26). Only by careful prearrangement of the conformation of the entering PG monomer unit can the required proximities of stems of adjacent glycan strands be met with high probability. We have argued that blocking reading of the template is one mode of action for oritavancin and other vancomycin-like glycopeptides (3, 5).

Lattice models for the PG of *S. aureus* are in their infancy (26). Nevertheless, incorporating PG repeat units with mixed geometries (bridge lengths of 5 and 1 glycyl units, for example, or even 3 and 1 units) is hard to envision. At the very least, model building of the PG lattice would be vastly more complicated if such hybrids were possible. Unambiguous elimination of the hybrid-lattice possibility is therefore crucial to lattice model building and is the focus of this report.

MATERIALS AND METHODS

Bacterial strains and growth conditions. Strains used are listed in Table 1. Starter cultures of the strains were prepared by inoculating 5 ml of Trypticase soy broth (TSB) in a test tube with a single colony obtained from a nutrient agar plate. The starter cultures were shaken at 200 rpm in an Environ-Shaker (Lab-Lines Instruments, Inc., Melrose Park, IL),

Received 14 August 2012 Accepted 10 January 2013
Published ahead of print 18 January 2013
Address correspondence to Jacob Schaefer, jschaefer@wustl.edu.
This publication is dedicated to Harald Labischinski, a friend and colleague who passed away in August 2010.
Supplemental material for this article may be found at http://dx.doi.org/10.1128/JB.01471-12.

doi:10.1128/JB.01471-12

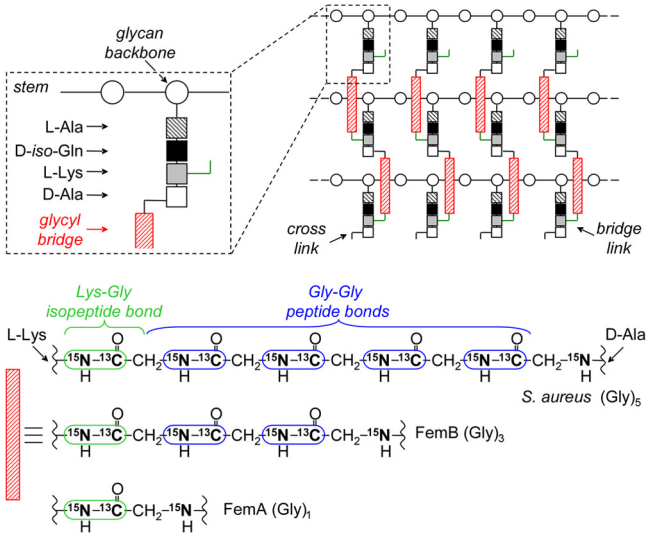

FIG 1 (Top) Schematic representation of an idealized peptidoglycan of *S. aureus* and its Fem mutants. A tetrapeptide stem, L-Ala–D-*iso*-Glu–L-Lys–D-Ala (squares), is attached to every second sugar of the glycan backbone (circles). The numbers of glycyl residues in the bridging segment (red rectangles) are 5 (*S. aureus*), 3 (FemB mutant), and 1 (FemA mutant). (Bottom) Label distribution in the PG-bridging segment for growth in defined medium containing L-[ε-^{15}N]lysine and [1-^{13}C,^{15}N]glycine.

maintained overnight at 37°C. The starter culture grown overnight (1% final volume) was added to 2 liters of sterile *S. aureus* standard medium (SASM) (25, 27). Six 1-liter flasks each contained 330 ml SASM and the following components on a per-liter basis: 10 g of D-(+)-glucose; 1 g each of $K_2HPO_4 \cdot 3H_2O$, KH_2PO_4, and $(NH_4)_2SO_4$; 0.2 g of $MgSO_4 \cdot 7H_2O$; 10 mg each of $MnSO_4 \cdot H_2O$, $FeSO_4 \cdot H_2O$, and NaCl; 5 mg each of adenine, cytosine, guanine, uracil, and xanthine; 2 mg each of thiamine-HCl (vitamin B_1), niacin (vitamin B_3), and calcium pantothenate (vitamin B_5); 1 mg each of riboflavin (vitamin B_2), pyridoxine-HCl (vitamin B_6), inositol, $CuSO_4 \cdot 5H_2O$, and $ZnSO_4 \cdot 7H_2O$; 0.1 mg each of biotin (vitamin B_7) and folic acid (vitamin B_9); and 0.1 g of all 20 common amino acids. The pH of SASM was adjusted to 7.0 with 1 M KOH, followed by sterile filtration (0.22-μm membrane).

The natural-abundance amino acids in SASM were replaced by either [1-^{13}C]glycine or [1-^{13}C,^{15}N]glycine (Isotec, Inc.) and L-[ε-^{15}N]lysine (Cambridge Isotope Laboratories, Inc.) to incorporate specific ^{13}C and ^{15}N labels in the bridging segment in the PG of intact cells (Fig. 1). Typically, cells were harvested during log-phase growth at an optical density at 660 nm (OD_{660}) of 0.6 by centrifugation at 10,000 × *g* for 10 min at 4°C in a Sorvall GS-3 rotor. Cell pellets were rinsed twice with 300 ml of ice-cold 40 mM triethanolamine hydrochloride (pH 7.0, adjusted with 1 M NaOH). The rinsed pellets were resuspended in 15 ml of the same buffer, followed by rapid freezing and lyophilization. The resulting lyophilized intact cells harvested from 2 liters of growth typically weighed 400 mg.

Isolation of peptidoglycan. Isolated cell walls were prepared from lyophilized intact cells, as previously described (25). Briefly, lyophilized cells from 2 liters of log-phase growth were resuspended in 100 ml of sterile 0.025 M potassium phosphate buffer (pH 7.0), boiled for 30 min, and then chilled in an ice bath. DNase I (type II, from bovine pancreas; Sigma-Aldrich) (1 mg per 100 mg cells [dry weight]) was added to the cell suspension, and the mixture was transferred into a 250-ml Bead-Beater (Biospec Products, Bartlesville, OK) chamber filled to one-third with 0.5-mm-diameter glass beads. Cell disruption employed 10 1-min cycles separated by 1-min cooling periods at 0°C. Glass beads were separated from the broken cells with a coarse sintered glass funnel. The cells were washed with 1 liter of 10 mM EDTA. Centrifugation of the filtrate at 10,000 × *g* for 1 h at 4°C provided crude cell walls.

The crude cell wall pellets were resuspended in a sterile 10 mM triethanolamine hydrochloride buffer (pH 7.0, adjusted with 1 M NaOH), to which 100 ml of boiling 4% sodium dodecyl sulfate (SDS) was added dropwise with continuous stirring. After boiling for 30 min, the suspension was allowed to cool for 2 h with stirring, after which it was allowed to stand unstirred overnight at room temperature and sedimented by centrifugation at 38,000 × *g* for 1 h at room temperature in a Sorvall SS-34 rotor. SDS was removed by rinsing the cell walls with 100 ml of triethanolamine buffer at least four times, with centrifugation after each rinse, until no SDS could be observed. The pellet was resuspended in 60 ml of 0.01 M Tris buffer (pH 8.2) containing 1 mg per 100 mg cells (dry weight) of DNase I and 3.2 mg per 100 mg cells (dry weight) of trypsin (type II-S, from bovine pancreas; Sigma-Aldrich) and α-chymotrypsin (type II, from bovine pancreas; Sigma-Aldrich). The suspension was incubated at 37°C, shaken at 150 rpm in an Environ-Shaker for 16 h, and then sedimented at 38,000 × *g* for 1 h at 20°C and washed at least four times with buffer, with centrifugation after each rinse. Cell walls were then resuspended in 10 ml of the triethanolamine buffer, followed by rapid freezing and lyophilization. The resulting isolated cell walls weighed approximately 150 mg. Cell wall isolation for all bacterial strains was processed under identical conditions.

Electron microscopy. Starter cultures of wild-type *S. aureus* (BB255) and its FemA mutants grown in TSB overnight were used to inoculate 40 ml of sterile SASM (1% final volume) in 125-ml flasks. Cells were grown at 37°C, shaken at 200 rpm in an Environ-Shaker, and harvested at log phase at an OD_{660} of 0.2 by centrifugation at 2,750 × *g* for 20 min at 4°C (Eppendorf 5810R centrifuge). For ultrastructural analysis, bacteria were fixed in 1 ml of 2% paraformaldehyde–2.5% glutaraldehyde (Polysciences, Inc.) in 100 mM phosphate buffer (pH 7.2) for 3 h at room temperature. Samples were washed in phosphate buffer and postfixed in 1% osmium tetroxide (Polysciences, Inc.) for 1 h. Samples were then rinsed extensively in distilled water prior to *en bloc* staining with 1% aqueous uranyl acetate (Ted Pella, Inc.) for 1 h. Following several rinses in distilled water, samples were dehydrated in a graded series of ethanol and embedded in Eponate 12 resin (Ted Pella, Inc.). Sections of 95 nm were cut with a Leica Ultracut UCT ultramicrotome (Leica Microsystems, Inc.), stained with uranyl acetate and lead citrate, and viewed on a Jeol 1200 EX transmission electron microscope (Jeol USA, Inc.).

Solid-state nuclear magnetic resonance (NMR) samples. The intact-cell and isolated cell wall samples were obtained from the same growth to exclude variation in growth of the mutants from batch to batch. The intact-cell spectra were scaled according to sample weight and total number of scans (see the supplemental material). As for the isolated cell wall spectra, because residual broken glass beads from cell isolation could contribute to the sample weight, the spectra were normalized with respect to the natural-abundance aliphatic-carbon peak heights. However, all cell wall isolations were processed under identical conditions so that normalization to weight and scans or normalization to peak height gave the same results (see the supplemental material).

TABLE 1 *Staphylococcus aureus* strains and their sensitivity to methicillin

Strain	Description	Relevant genotype	MIC (μg/ml) of methicillin[a]	Reference(s)
BB255	Wild type	NCTC 8325	0.75	1, 2
BB270	Isogenic MRSA	NCTC 8325 *mec*	6.00	1, 2
UT34-2	FemB	NCTC 8325 *mec* Ω2006 (*femB*::Tn*551*)	0.75	12
UK17	FemA	NCTC 8325 *mec* Δ*femA* (*ochre*)	0.19	8, 14
AS145	FemAB	NCTC 8325 *mec* Δ*femAB*::*tetK*	0.016	16, 23

[a] MIC data obtained from references 3, 22, and 24.

NMR spectrometers. Experiments were performed on intact cells at 7.0 tesla (T) (300 MHz for ^{1}H, 75 MHz for ^{13}C, and 30 MHz for ^{15}N) and on isolated cell walls at 4.7 T (200 MHz for ^{1}H, 50 MHz for ^{13}C, and 20 MHz for ^{15}N), provided by 89-mm-bore Oxford (Cambridge, United Kingdom) superconducting solenoids. The four-frequency transmission line probe used in the 7.0-T spectrometer had a 14-mm-long, 9-mm-inner-diameter sample coil, while the one used in the 4.7-T spectrometer had a 17-mm-long, 8.6-mm-inner-diameter sample coil. Both probes were equipped with a Chemagnetics/Varian magic-angle spinning ceramic stator, and samples were spun at room temperature at 5 kHz (maintained within ±2 Hz). Radiofrequency pulses were produced by 1-kW Kalmus, ENI, and American Microwave Technology power amplifiers, each under active control; π-pulse lengths were 10 μs for ^{13}C and ^{15}N. Proton-carbon- and proton-nitrogen-matched cross-polarization transfers were done at 50 kHz for 2 ms. Proton dipolar decoupling during signal acquisition was done at 105 kHz (for the 7.0-T spectrometer) and 98 kHz (for the 4.7-T spectrometer). Spectra typically resulted from acquisition of 4,098 scans (intact cells) and 20,480 scans (isolated cell walls). For all spectra, the uncertainty in the integrated intensities was less than 1% (25).

Experiments performed at 12 T used a six-frequency transmission line probe having a 12-mm-long, 6-mm-inner-diameter analytical coil and a Chemagnetics/Varian ceramic spinning module. Samples were spun by using a thin-wall Chemagnetics/Varian (Fort Collins, CO) 5-mm-outer-diameter zirconia rotor at 7,143 Hz, with the speed under active control and maintained to within ±2 Hz. A Tecmag Libra pulse programmer (Tecmag, Houston, TX) controlled the spectrometer. A 2-kW American Microwave Technology power amplifier was used to produce radiofrequency pulses for ^{13}C (125 MHz). The ^{1}H (500-MHz) radiofrequency pulses were generated by a 2-kW Creative Electronics tube amplifier driven by a 50-W American Microwave Technology power amplifier. All final-stage amplifiers were under active control. The π-pulse lengths were 9 μs for ^{13}C and ^{1}H. Proton-carbon-matched cross-polarization transfers were made in 2 ms at 56 kHz. Proton dipolar decoupling was done at 100 kHz during data acquisition.

REDOR analysis. Rotational-echo double-resonance (REDOR) ^{13}C{^{15}N} solid-state NMR (25, 28) was used to measure the PG glycine content in intact cells and isolated cells walls of Fem mutants. ^{13}C{^{15}N} REDOR restores the dipolar coupling between heteronuclear pairs of spins, e.g., ^{13}C and ^{15}N spins in a peptide bond, which is removed by magic-angle spinning. REDOR experiments are always performed in two parts (28): once without (S_0) and once with (S) rotor-synchronized dephasing pulses. In the first part of the experiment (S_0), magic-angle spinning averages chemical shift and dipolar-anisotropic interactions to produce an isotropic signal of full intensity. In the second part (S), the dephasing pulses applied periodically restore the dipolar coupling, thereby dephasing, or reducing, the observed signal. The difference in signal intensity ($\Delta S = S_0 - S$) for the observed spin leads to a direct quantitative measurement of the internuclear distance between the observed and dephasing spins (28). For magic-angle spinning at 5 kHz, the total dephasing, and therefore ΔS, reaches a maximum value after 8 rotor periods for the 1.2-kHz one-bond ^{13}C-^{15}N dipolar coupling in a peptide bond (25). REDOR line shapes and resolution are determined by distributions of isotropic shifts. REDOR spectra obtained at 4.7, 7, and 12 T therefore appear the same.

TEDOR. Transferred-echo double resonance (TEDOR) (29, 30) was used for selective detection of cell walls in whole cells of the FemA mutant. This experiment begins with a ^{1}H→^{15}N cross-polarization transfer and observable ^{15}N magnetization (S_x). Next, a 12-T_r ^{15}N{^{13}C} REDOR sequence establishes nonobservable ^{15}N^{13}C (S_yI_z) bilinear coherence, which is transformed into ^{13}C^{15}N (S_zI_y) bilinear coherence by a pair of coincident ^{13}C and ^{15}N 90° pulses (29). A 12-T_r ^{13}C{^{15}N} REDOR sequence then creates observable ^{13}C magnetization (I_x) only for those ^{13}C's which are directly bonded to ^{15}N.

In the double-labeled cell walls, the great majority of these ^{13}C's are at the bridge link connecting the ε-lysine ^{15}N-labeled amine (99% isotopically enriched) to the glycine ^{13}C-labeled carbonyl carbon (50% isotopically enriched). There are 8 other ^{15}N-^{13}C amine-carbonyl bonds in the PG repeat unit (Fig. 1), but these are all at natural abundance (^{15}N, 0.37%; ^{13}C, 1.1%) and hence contribute only (8)(0.0037)(0.011) = 0.00033, compared to 0.5 relative intensity units for the bridge link, a factor of 1,500. Inclusion of the amine-carbonyl bonds of teichoic acids reduces this bridge link factor by one-half (1,500/2 = 750); that is, the natural-abundance contribution to the TEDOR-generated ^{13}C magnetization in isolated cell walls is about 0.13% (1/750).

The natural-abundance peptide component of the cytoplasmic proteins of the intact cell is typically 5 times that of the PG, which means that compared to the bridge link, an additional (40)(0.0037)(0.011) = 0.0016 relative intensity units must be included for a total of 0.00226 and a bridge link factor of 221. The natural-abundance contribution to the TEDOR-generated ^{13}C magnetization in intact cells is therefore about 0.5%.

For labeled glycines in the cytoplasmic protein (5% of the total), we estimate the relative intensity units contributing to the TEDOR-generated magnetization as (40)(0.05)(0.0037)(0.5) = 0.0037, which translates into a total contribution from PG and cytoplasmic proteins of 0.0023 + 0.0037 = 0.0060 relative intensity units and a bridge link factor of 83; that is, the total non-bridge-link contribution to the TEDOR-generated ^{13}C magnetization in whole cells is 1.2%, and that in isolated cell walls, as described above, is 0.13%.

The full-echo (S_0) spectrum of ^{15}N→^{13}C TEDOR after 840 ms for isolated cell walls of the FemA mutant labeled with [1-^{13}C,^{15}N]glycine and L-[ε-^{15}N]lysine was deconvoluted by using a customized Matlab program (MathWorks, Inc.). The deconvolution parameters were based on a peak with a Lorentzian-to-Gaussian line shape ratio of 0.5 and a fixed line width of 180 Hz. Spectra were fit by minimizing the residual sum of squares and optimized for an uncorrected R^2 value greater than 0.995. The peak intensity ratio was determined by numerical integration. For the isolated cell wall spectrum, the fitted individual peak positions and relative peak intensities (shown in parentheses) are 169.1 ppm (0.885) and 165.6 ppm (0.650), with a peak intensity ratio of 0.58. A similar analysis was performed on the intact-cell REDOR spectrum (see the supplemental material).

CODEX. Center-band-only detection of exchange (CODEX) (26) was used together with TEDOR-generated bridge link magnetization to search for ^{13}C-^{13}C exchange during a mixing time of 840 ms. Only ^{13}C's with net polarization before the mixing time can exchange, and these carbons must have distinct isotropic chemical shifts. Thus, the exchange is limited to ^{13}C's directly bonded to ^{15}N's (see the supplemental material). The TEDOR and CODEX experiments were performed exclusively at 12 T.

Mass spectrometry. Cells grown in unlabeled SASM were digested into muropeptides with lysozyme and mutanolysin, as previously described (31). Briefly, cells were incubated for 4 h at 37°C with mutanolysin (1 μg/μl) (from *Streptomyces globisporus* ATCC 21553, lyophilized powder, 5 kilounits; Sigma-Aldrich) and lysozyme (1 μg/μl) (from chicken egg white; Sigma-Aldrich). The suspension was boiled for 5 min, and the supernatants were collected by centrifugation at 10,000 × *g* for 5 min.

Liquid chromatography-mass spectrometry (LC-MS) and tandem mass spectrometry (MS-MS) were performed by using a PicoView PV-500 (New Objective, Woburn, MA) nanospray stage attached to either an LTQ-FT mass spectrometer or an LTQ-Orbitrap mass spectrometer (ThermoFisher, San Jose, CA).

Muropeptide samples were loaded into an uncoated 75-μm-inner-diameter fused-silica capillary column with a 15-μm PicoFrit tip (New Objectives, Woburn, MA), packed with C_{18} reverse-phase material (3 μm, 100 Å; Phenomenex, Torrance, CA) for 15 cm. The column was eluted at a flow rate of 250 nl/min for 10 min with 0.1% (vol/vol) formic acid in water and subsequently with a 60-min linear acetonitrile gradient (0% to 40%) with 0.1% formic acid. The samples, as they emerged from the column, were sprayed into a 209 LTQ-FT mass spectrometer. Full mass

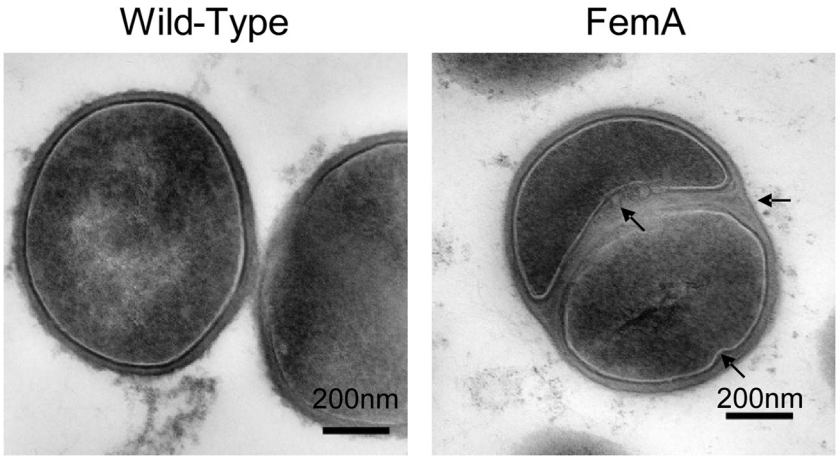

FIG 2 Transmission electron micrographs of intact cells of methicillin-resistant *S. aureus* (BB255) and the FemA mutant grown in defined medium and harvested at an optical density at 660 nm of 0.2. Arrows indicate morphological irregularities.

spectra were recorded in the Fourier transform (FT) component of the instrument at a resolving power of 100,000 (at *m/z* 400).

Accurate-mass product-ion spectra of muropeptides were acquired by introducing the samples by nanospray as they eluted from the liquid chromatograph to an LTQ-Orbitrap mass spectrometer. To obtain major-component product-ion spectra, cycles consisting of one full FT scan mass spectrum and five ensuing data-dependent MS-MS scans acquired by the Orbitrap instrument (with a normalized collision energy setting of 35%) were repeated continuously throughout the elution, with the following dynamic exclusion settings: repeat count of 3, repeat duration of 15 s, and exclusion duration of 30 s.

RESULTS AND DISCUSSION

Transmission electron micrographs. Figure 2 shows the transmission electron micrographs (TEMs) of ultrathin sections of wild-type *S. aureus* (BB255) and the FemA (UK17) mutant. The FemA mutant exhibits a defective bacterial cell wall, indicated by the arrows in Fig. 2 (right), with partial cell wall thickening and diffused staining at cross walls. This suggested an accumulation of immature peptidoglycan at the septum, in association with an aberrant growth (17, 25). A similar irregular morphology was also observed for the FemB mutant (25).

Labeling strategy. An accurate number of glycine residues in the PG bridges of intact cells was determined by labeling the PG with L-[ϵ-^{15}N]lysine and [1-^{13}C,^{15}N]glycine. Lysine does not scramble, and the glycine isotopic enrichments in the cell wall of Fem mutants are constant (25). The REDOR difference (ΔS^{total}) selects the peptide-bonded ^{13}C-^{15}N spin pairs, both *iso*-Lys-Gly and Gly-Gly peptide bonds, primarily from the bacterial cell wall (25). An isopeptide bond between L-[ϵ-^{15}N]lysine and [1-^{13}C]glycine, shown in Fig. 1 (bottom, green), is unique to the cell wall PG and does not occur in proteins. The contribution from Gly-Gly peptide bonds in proteins (see Materials and Methods) is minimal in intact cells (25) and is absent in isolated cell walls.

In the ΔS^{total} spectra of intact cells (25) and isolated cell walls of the FemA mutant (Fig. 3), the peaks due to un-cross-linked (open) glycyl bridges are partially resolved at 165 ppm from those due to the cross-linked (closed) glycyl bridges at 171 ppm. The ΔS integrated intensities, instead of peak heights (25), were used for the correct comparative analysis of cell wall compositions in Fem mutants. The use of integrated intensities is important to take into account the asymmetric line shape of the FemA peak (Fig. 3, blue). The 171-ppm ΔS^{total} integrated intensities of wild-type *S. aureus* (BB255) for both intact cells and isolated cell walls were normalized to 5.0 glycine-equivalent units (GEU) (25).

PG heterogeneity determined by REDOR NMR. For isolated cell walls of FemB and FemA mutants, the measured PG glycine contents determined from the 171-ppm ΔS^{total} integrated intensities (Fig. 3, right) were 3.1 ± 0.1 GEU (FemB) and 1.0 ± 0.1 GEU (FemA), respectively. This indicates that the isolated cell walls of Fem mutants have the expected uniform composition, consisting entirely of triglycyl bridges for the FemB mutant and monoglycyl bridges for the FemA mutant. In contrast, the PG glycine content in intact cells was reduced to 2.6 ± 0.1 GEU for the FemB mutant and was increased to 1.3 ± 0.1 GEU for the FemA mutant. We attribute these differences to the presence of PG fragments with various glycyl bridge lengths. Pentaglycyl bridge biosynthesis in *S. aureus* can build bridges only in increments of 1, 3, and 5 glycine residues (9–11). Therefore, a reduction in the PG glycine content of 16% in intact cells of the FemB mutant indicates that a signifi-

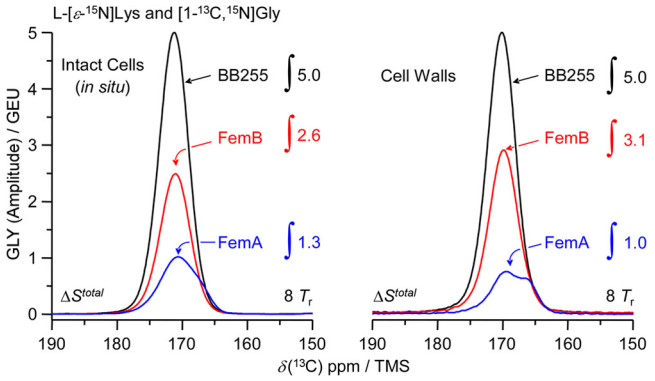

FIG 3 ^{13}C{^{15}N} REDOR difference spectra (ΔS^{total}) after eight rotor periods (8 T_r) with 5-kHz magic-angle spinning of methicillin-resistant *S. aureus* BB255, the FemB mutant, and the FemA mutant labeled by [1-^{13}C,^{15}N]glycine and L-[ϵ-^{15}N]lysine. The 171-ppm ΔS^{total} integrated intensities of BB255 were set equal to 5.0 GEU. (Left) Intact-cell spectra at 75 MHz (for details, see reference 29). (Right) Cell wall spectra at 50 MHz (for details, see Fig. S3 in the supplemental material). TMS, tetramethylsilane.

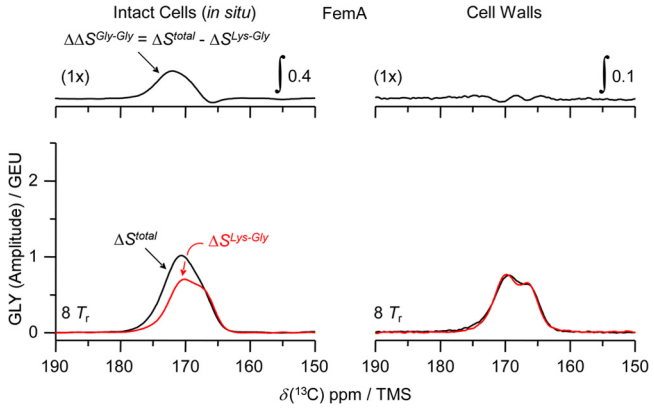

FIG 4 $^{13}C\{^{15}N\}$ REDOR spectra after eight rotor periods (8 T_r) with 5-kHz magic-angle spinning of the FemA mutant labeled with L-[ϵ-^{15}N]lysine and either [1-^{13}C,^{15}N]glycine (ΔS^{total}) (black) or [1-^{13}C]glycine ($\Delta S^{Lys-Gly}$) (red). Intact-cell spectra at 75 MHz are shown on the right, and cell wall spectra at 50 MHz are shown on the left. (Top) Difference spectra, $\Delta\Delta S^{Gly-Gly} = \Delta S^{total} - \Delta S^{Lys-Gly}$. (Bottom) Overlaid ΔS^{total} and $\Delta S^{Lys-Gly}$ spectra. For further details, see Fig. S4 in the supplemental material.

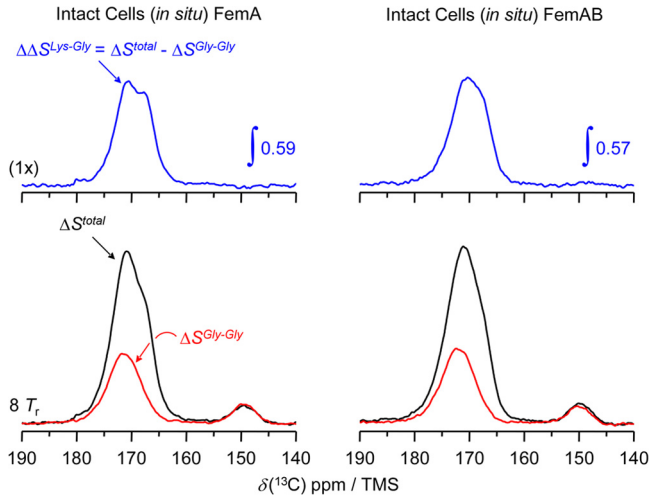

FIG 5 Intact-cell $^{13}C\{^{15}N\}$ REDOR spectra at 50 MHz after eight rotor periods (8 T_r) with 5-kHz magic-angle spinning of the FemA mutant (left) and the FemAB null mutant (right) labeled with L-[ϵ-^{15}N]lysine and either [1-^{13}C,^{15}N]glycine (ΔS^{total}) or [1-^{13}C,^{15}N]glycine ($\Delta S^{Gly-Gly}$). (Top) Difference spectra, $\Delta\Delta S^{Lys-Gly} = \Delta S^{total} - \Delta S^{Gly-Gly}$. (Bottom) Overlaid ΔS^{total} and $\Delta S^{Gly-Gly}$ spectra.

cant portion of PG units have monoglycyl bridges (see Table S1 in the supplemental material). An increase in the PG glycine content of 30% in the intact cells of the FemA mutant suggests a heterogeneous mixture of PG units with mono-, tri-, and/or pentaglycyl bridges.

To display the likely presence of a heterogeneous mixture of PG fragments in intact cells of the FemA mutant more directly, we removed the isopeptide bond contribution from the ΔS^{total} integrated intensity. This was achieved by the spectral subtraction of $\Delta S^{Lys-Gly}$, the $^{13}C\{^{15}N\}$ REDOR difference of intact cells labeled with L-[ϵ-^{15}N]lysine and [1-^{13}C]glycine, from ΔS^{total}. Figure 4 (bottom) shows the overlaid ΔS^{total} (black) and $\Delta S^{Lys-Gly}$ (red) spectra. The difference spectra (Fig. 4, top), $\Delta\Delta S^{Gly-Gly} = \Delta S^{total} - \Delta S^{Lys-Gly}$, are exclusively from the putative PG Gly-Gly bonds. In the $\Delta\Delta S^{Gly-Gly}$ spectra (Fig. 4, top), a peak centered at approximately 174 ppm is clearly visible for intact cells of the FemA mutant, with an intensity of 0.4 GEU (top left). This peak is absent for isolated cell walls (Fig. 4, top right). Assuming only a triglycyl residue contribution, the estimated number of PG units not associated with monoglycyl bridges is ~10%. In contrast, the $\Delta\Delta S^{Gly-Gly}$ in isolated cell walls is zero, which indicates that the PG is uniform, consisting entirely of monoglycyl-PG units.

A similar analysis performed on the FemB mutant (Table 1; see also details in Fig. S3 and S4 in the supplemental material) revealed a decrease of the glycine content in intact cells, which may be due to the presence of monoglycyl bridges, but no decrease in isolated cell walls.

PG heterogeneity in the FemAB mutant determined by REDOR NMR. To confirm that the presence of a heterogeneous PG fragment mixture in intact cells of the FemA mutant is not due to leakage of the point mutation (16, 17), we characterized the glycine content in intact cells of the FemAB null mutant and compared the results with those for the FemA mutant. The FemAB null mutant was constructed by a complete inactivation of both the *femA* and *femB* genes (20, 21). Figure 5 (bottom) shows the overlaid $\Delta S^{Lys-Gly}$ (red line) and ΔS^{total} (black line) spectra. The difference spectra (Fig. 5, top), $\Delta\Delta S^{Lys-Gly} = \Delta S^{total} - \Delta S^{Lys-Gly}$, are exclusively from the ^{13}C glycyl-carbonyl carbons that are directly bonded to the ϵ-^{15}N of lysine found only in PG. The integrated intensities of $\Delta\Delta S^{Lys-Gly}$ are 0.59 for the FemA mutant and 0.57 for the FemAB mutant. Comparable $\Delta\Delta S^{Lys-Gly}$ values for both the FemA and FemAB mutants indicate a similar PG composition. The observed $\Delta S^{Lys-Gly}$ contribution can occur only from Gly-Gly peptide bonds in PG, with significant PG heterogeneity in intact cells of both the FemA and FemAB mutants. Because of complete *femA* and *femB* inactivation in the FemAB mutant, other enzymes must be active in forming Gly-Gly bonds (see Discussion).

Confirmation of PG heterogeneity by TEDOR-CODEX NMR. A TEDOR-CODEX NMR experiment was used to examine directly the homogeneity of the peptidoglycan of intact FemA cells and isolated cell walls labeled by [1-^{13}C]glycine and [ϵ-^{15}N]lysine.

A comparison of the TEDOR-generated bridge link magnetization for intact cells and isolated cell walls labeled by [1-^{13}C]glycine and [ϵ-^{15}N]lysine is made in Fig. 6 (bottom left). The spectra have been normalized to the 165-ppm peak. This normalization makes the assumption that in isolating the cell walls, all the PG was retained, including the partially cross-linked nascent layer and, therefore, all of the unique amine-terminated bridges that contribute to the 165-ppm peak. The deconvoluted TEDOR spectrum of the isolated cell walls provides a quantitative measurement of open (165-ppm peak) (Fig. 6, bottom left, green peak) and closed (171-ppm peak) (Fig. 6, bottom left, blue peak) bridge links in PG (see details in Fig. S6a in the supplemental material). The deconvoluted closed-to-open peak intensity ratio is 0.58 for isolated cell walls, which is in good agreement with the experimentally determined PG cross-link density of 0.62 (25). The intact-cell signal intensity centered near 171 ppm (Fig. 6, bottom left, red spectrum) is ~10% higher than the corresponding cell wall signal intensity. This difference is an order of magnitude higher than the intact-cell non-bridge-link contributions to the 171-ppm signal (see Materials and Methods) and is consistent only with the presence of nonmonoglycyl bridges. These bridges contribute to the

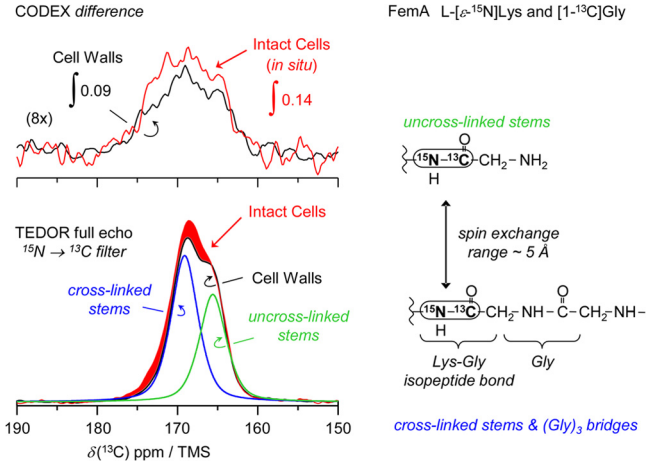

FIG 6 TEDOR-CODEX ^{13}C spectra after 12 rotor periods (12 T_r) obtained at 125 MHz with 7,143-Hz magic-angle spinning for FemA mutant cells labeled with L-[ε-^{15}N]lysine and [1-^{13}C]glycine. TEDOR full-echo spectra are shown at the bottom, and CODEX difference spectra (after a mixing time of 840 ms) are shown at the top. Spectra of intact cells are shown in red, and isolated cell walls are shown in black. The spectra are the result of the accumulation of 1,180,000 scans for intact cells and 475,000 scans for isolated cell walls. Deconvoluted TEDOR spectra showing open (165-ppm peak) (green) and closed (171-ppm peak) (blue) bridge links in peptidoglycan are shown at the bottom. Fitted individual peak positions and relative integrated peak intensities (shown in parentheses) for the isolated cell wall spectrum are 169.1 ppm (0.885) and 165.6 ppm (0.650). For further details, see Fig. S6a in the supplemental material.

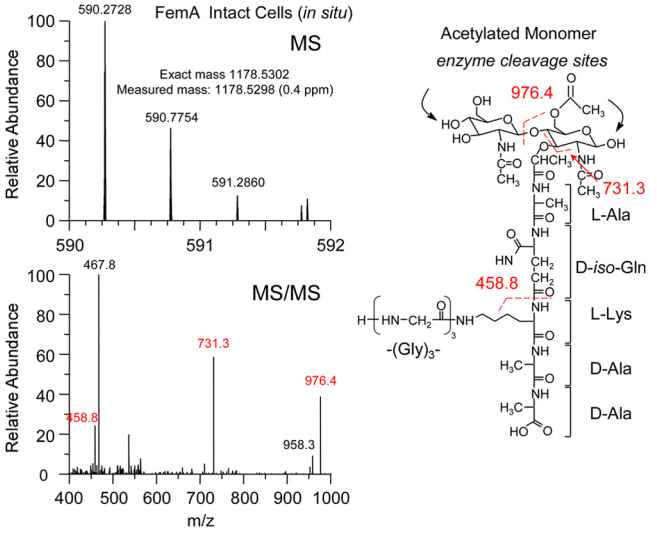

FIG 7 Mass spectra of the acetylated muropeptide (structure shown on the right) from the FemA mutant containing triglycyl bridge residues. The accurate-mass measurement deviates by 0.4 ppm from the theoretical mass. The bottom panel shows the product-ion spectrum of the parent ion. The proposed structures of the fragments are shown in Fig. S7b in the supplemental material.

171-ppm peak but make no contribution to the 165-ppm peak of the TEDOR full-echo spectrum. The difference between the ~10%-higher glycine content of bridges from the TEDOR experiment and the 30% estimated in the REDOR experiment (Fig. 3), where all glycyl carbonyl carbons report instead of just those part of a Gly-Lys ^{13}C-^{15}N bond, means that these extra bridges are predominantly triglycyl residues.

The center-band-only detection-of-exchange part of the TEDOR-CODEX experiment used the TEDOR-generated bridge link magnetization to search for ^{13}C-^{13}C exchange during a mixing time of 840 ms (six rotor periods). Only ^{13}C's with net magnetization before the mixing time can exchange, and these carbons must have distinct isotropic chemical shifts (26). For FemA monoglycyl bridges, exchange can occur only between adjacent bridges that have glycyl carbonyl carbons within 5 Å. The most obvious exchange is between ^{13}C's with isotropic shifts of 171 and 165 ppm (Fig. 6, right), which corresponds to exchange between cross-linked and un-cross-linked stems, respectively. However, both peaks are heterogeneously broadened and consist of many different isotropic shifts arising from slight differences in local bridge conformation. Thus, exchange is possible between, for example, ^{13}C's in cross-linked stems with a shift of 170 ppm and those with a shift of 172 ppm. Details regarding the possible CODEX exchange pairs can be found in Fig. S6b in the supplemental material. The observed sizeable CODEX difference signal for FemA isolated cell walls (Fig. 6, top left, black spectrum), which have a uniform composition of monoglycyl bridges, indicates that many stems are necessarily incorporated into a tight-lattice structure.

Because the CODEX difference signal is greater for intact cells than for isolated cell walls (Fig. 6, top left), the triglycyl bridges must also be incorporated into some sort of a lattice or aggregate with proximity to other triglycyl and/or monoglycyl bridges. This extra lattice is apparently a relatively low-molecular-weight species that is, for the most part, lost in the cell wall isolation.

Confirmation of triglycyl bridges in FemA PG by mass spectrometry. The presence of PG heterogeneity was also investigated by using LC-MS analysis on the supernatant from the muramidase-digested intact cells of the FemA and FemB mutants and parent strain BB255 (see Fig. S7a in the supplemental material). For the FemA mutant, we detected an un-cross-linked monomer species with an accurate-mass measurement corresponding to the exact mass of an acetylated 5-residue muropeptide with three glycine residues in the bridge. As shown in Fig. 7, the accurate mass of 1,178.5298 differs by only 0.4 ppm from the exact mass of 1,178.5302. The structure of this fragment was confirmed by MS-MS (Fig. 7, bottom), and the proposed structural fragments are shown in Fig. S7b in the supplemental material. We speculate that these FemA species exist primarily in a region that is either unfavorable for digestion or lost during sample preparation before mass spectrometric analysis, because yields of the triglycyl fragment (see Fig. S7a, red, in the supplemental material) were only 10% of those expected from the NMR analysis. Analysis of the FemB mutant showed primarily triglycyl subunits with some mono- and no pentaglycyl units (see Fig. S7a, green, in the supplemental material). LC-MS analysis was also performed on the supernatant of the muramidase-digested FemAB null mutant (data not shown), but no tri- or pentaglycyl subunits were detected (17, 21). This unexpected result suggests sequestration in regions even more unfavorable for digestion than those for the FemA mutant.

Origin of heterogeneity in Fem mutants. PG heterogeneity in the intact cells of the FemA mutant is present regardless of the construction of the *fem* mutant by single point mutation (16, 22) or complete inactivation of the *femA* and *femB* genes (20, 21). The presence of PG heterogeneity in the FemAB mutant rules out the

possibility that FemX or FemB is involved. We speculate that the PG heterogeneity is linked to an acquired hidden mutation(s) during cell construction (22) and is therefore associated with cell wall biosynthesis. The loss of heterogeneous PG fragments in the FemA mutant during cell wall isolation (Fig. 3 and 4) suggests that the PG units with predominantly triglycyl bridges are not incorporated with monoglycyl-PG units to form a mature cell wall. This may be due to the inability to form mixed cell wall architectures in template-based PG biosynthesis (3, 4). The heterogeneous material appears to be localized close to the membrane surface (Fig. 2, right) and may be responsible for irregular cell division and growth (25), prolonged doubling times (22), cell wall thickening (24), and aberrant cell shapes (24, 25). However, we believe that the regained susceptibility to β-lactam antibiotics in Fem mutants of MRSA (2, 12) is not related to the accumulation of immature cell wall fragments and abnormal cell division but rather is associated with the inability of PBP2a to cross-link short bridges to stems.

ACKNOWLEDGMENTS

We thank Brigitte Berger-Bächi (Universität Zürich, Institut für Medizinische Mikrobiologie, Switzerland) for providing the bacterial strains.

This work was supported in part by the National Institutes of Health under grant number EB002058. The mass spectrometry work was supported by grants from the National Center for Research Resources (grant number 5P41RR000954-35), now the National Institute of General Medical Sciences (grant number 8 P41 GM103422-35), of the National Institutes of Health.

REFERENCES

1. **Hakenbeck R, Coyette J.** 1998. Resistant penicillin-binding proteins. Cell. Mol. Life Sci. **54**:332–340.
2. **Labischinski H.** 1992. Consequences of the interaction of β-lactam antibiotics with penicillin-binding proteins from sensitive and resistant *Staphylococcus aureus* strains. Med. Microbiol. Immunol. **181**:241–265.
3. **Kim SJ, Cegelski L, Stueber D, Singh M, Dietrich E, Tanaka KSE, Parr TR, Jr, Far AR, Schaefer J.** 2008. Oritavancin exhibits dual mode of action to inhibit cell wall biosynthesis in *Staphylococcus aureus*. J. Mol. Biol. **377**: 281–293.
4. **Kim SJ, Matsuoka S, Patti GJ, Schaefer J.** 2008. Vancomycin derivative with damaged D-Ala-D-Ala binding cleft binds to cross-linked peptidoglycan in the cell wall of *Staphylococcus aureus*. Biochemistry **47**:3822–3831.
5. **Kim SJ, Schaefer J.** 2008. Hydrophobic side-chain length determines activity and conformational heterogeneity of a vancomycin derivative bound to the cell wall of *Staphylococcus aureus*. Biochemistry **47**:10155–10161.
6. **Kern T, Hediger S, Mueller P, Giustini C, Joris B, Bougault C, Vollmer W, Simorre J-P.** 2008. Toward the characterization of peptidoglycan structure and protein-peptidoglycan interactions by solid-state NMR spectroscopy. J. Am. Chem. Soc. **130**:5618–5619.
7. **Dmitriev BA, Toukach FV, Schaper K-J, Holst O, Rietschel ETT, Ehlers S.** 2003. Tertiary structure of bacterial murein: the scaffold model. J. Bacteriol. **185**:3458–3468.
8. **Seligman SJ, Pincus MR.** 1987. A model for the three-dimensional structure of peptidoglycan in staphylococci. J. Theor. Biol. **124**:275–292.
9. **Berger-Bächi B, Tschierske M.** 1998. Role of Fem factors in methicillin resistance. Drug Resist. Updat. **1**:325–335.
10. **Rohrer S, Berger-Bächi B.** 2003. FemABX peptidyl transferases: a link between branched-chain cell wall peptide formation and β-lactam resistance in gram-positive cocci. Antimicrob. Agents Chemother. **47**:837–846.
11. **Schneider T, Senn MM, Berger-Baechi B, Tossi A, Sahl H-G, Wiedemann I.** 2004. In vitro assembly of a complete, pentaglycine interpeptide bridge containing cell wall precursor (lipid II-Gly5) of *Staphylococcus aureus*. Mol. Microbiol. **53**:675–685.
12. **de Lencastre H, Jonge BLM, Matthews PR, Tomasz A.** 1994. Molecular aspects of methicillin resistance in *Staphylococcus aureus*. J. Antimicrob. Chemother. **33**:7–14.
13. **Rohrer S, Ehlert K, Tschierske M, Labischinski H, Berger-Bächi B.** 1999. The essential *Staphylococcus aureus* gene *fmhB* is involved in the first step of peptidoglycan pentaglycine interpeptide formation. Proc. Natl. Acad. Sci. U. S. A. **96**:9351–9356.
14. **Labischinski H, Ehlert K, Berger-Bächi B.** 1998. The targeting of factors necessary for expression of methicillin resistance in staphylococci. J. Antimicrob. Chemother. **41**:581–584.
15. **Henze U, Sidow T, Wecke J, Labischinski H, Berger-Bächi B.** 1993. Influence of *femB* on methicillin resistance and peptidoglycan metabolism in *Staphylococcus aureus*. J. Bacteriol. **175**:1612–1620.
16. **Ehlert K, Schröder W, Labischinski H.** 1997. Specificities of FemA and FemB for different glycine residues: FemB cannot substitute for FemA in staphylococcal peptidoglycan pentaglycine side chain formation. J. Bacteriol. **179**:7573–7576.
17. **Kopp U, Roos M, Wecke J, Labischinski H.** 1996. Staphylococcal peptidoglycan interpeptide bridge biosynthesis: a novel antistaphylococcal target? Microb. Drug Resist. **2**:29–41.
18. **Berger-Bächi B.** 1983. Insertional inactivation of staphylococcal methicillin resistance by Tn551. J. Bacteriol. **154**:479–487.
19. **Berger-Bächi B, Kohler ML.** 1983. A novel site on the chromosome of *Staphylococcus aureus* influencing the level of methicillin resistance: genetic mapping. FEMS Microbiol. Lett. **20**:305–309.
20. **Hübscher J, Jansen A, Kotte O, Schäfer J, Majcherczyk PA, Harris LG, Bierbaum G, Heinemann M, Berger-Bächi B.** 2007. Living with an imperfect cell wall: compensation of *femAB* inactivation in *Staphylococcus aureus*. BMC Genomics **8**:307. doi:10.1186/1471-2164-8-307.
21. **Strandén AM, Ehlert K, Labischinski H, Berger-Bächi B.** 1997. Cell wall monoglycine cross-bridges and methicillin hypersusceptibility in a *femAB* null mutant of methicillin-resistant *Staphylococcus aureus*. J. Bacteriol. **179**:9–16.
22. **Ling B, Berger-Bächi B.** 1998. Increased overall antibiotic susceptibility in *Staphylococcus aureus femAB* null mutants. Antimicrob. Agents Chemother. **42**:936–938.
23. **Billot-Klein D, Shlaes D, Bryant D, Bell D, van Heijenoort J, Gutmann L.** 1996. Peptidoglycan structure of *Enterococcus faecium* expressing vancomycin resistance of the VanB type. Biochem. J. **313**:711–715.
24. **Giesbrecht P, Kersten T, Maidhof H, Wecke J.** 1998. Staphylococcal cell wall: morphogenesis and fatal variations in the presence of penicillin. Microbiol. Mol. Biol. Rev. **62**:1371–1414.
25. **Sharif S, Kim SJ, Labischinski H, Schaefer J.** 2009. Characterization of peptidoglycan in Fem-deletion mutants of methicillin-resistant *Staphylococcus aureus* by solid-state NMR. Biochemistry **48**:3100–3108.
26. **Sharif S, Singh M, Kim SJ, Schaefer J.** 2009. *Staphylococcus aureus* peptidoglycan tertiary structure from carbon-13 spin diffusion. J. Am. Chem. Soc. **131**:7023–7030.
27. **Tong G, Pan Y, Dong H, Pryor R, Wilson GE, Schaefer J.** 1997. Structure and dynamics of pentaglycyl bridges in the cell walls of *Staphylococcus aureus* by ^{13}C-^{15}N REDOR NMR. Biochemistry **36**:9859–9866.
28. **Gullion T, Schaefer J.** 1989. Detection of weak heteronuclear dipolar coupling by rotational-echo double-resonance nuclear magnetic resonance. Adv. Magn. Reson. **13**:57–83.
29. **Hing AW, Vega S, Schaefer J.** 1992. Transferred-echo double-resonance NMR. J. Magn. Reson. A **96**:205–209.
30. **Hing AW, Vega S, Schaefer J.** 1993. Measurement of heteronuclear dipolar coupling by transferred-echo double-resonance NMR. J. Magn. Reson. A **103**:151–162.
31. **Patti GJ, Chen J, Gross ML.** 2009. Method revealing bacterial cell-wall architecture by time-dependent isotope labeling and quantitative liquid chromatography/mass spectrometry. Anal. Chem. **81**:2437–2445.